Research Article | Vol. 26, No. 4 | 19 Feb 2018 | OPTICS EXPRESS 4346

Optics EXPRESS

Spectrally shaping high-temperature radiators for thermophotovoltaics using Mo-HfO_2 trilayer-on-substrate structures

ETIENNE BLANDRE,[1,*] MAKOTO SHIMIZU,[1,2] ASAKA KOHIYAMA,[2] HIROO YUGAMI,[2] PIERRE-OLIVIER CHAPUIS,[1] AND RODOLPHE VAILLON [1,3]

[1] *Univ Lyon, CNRS, INSA-Lyon, Université Claude Bernard Lyon 1, CETHIL UMR5008, F-69621, Villeurbanne, France*

[2] *Graduate School of Engineering, Tohoku University, Aoba 6-6-01 Aramaki, Aoba-ku, Sendai 980-8579, Japan*

[3] *Radiative Energy Transfer Lab, Department of Mechanical Engineering, University of Utah, Salt Lake City, UT 84112, USA*

[*] *etienne.blandre@insa-lyon.fr*

Abstract: Easy-to-fabricate, high-temperature, thermally-stable radiators are critical elements for developing efficient and sustainable thermophotovoltaic energy conversion devices. In this frame, a trilayer-on-substrate structure is selected. It is composed of a refractory metal - molybdenum - constituting the substrate and an intermediate thin film sandwiched between two hafnia transparent layers. An in-depth analysis shows that two spectrally distinct interference regimes take place in the hafnia layer-molybdenum thin film substructure, and that backward and forward thermally-emitted waves by the thin film are selected in two distinct interferential resonating cavities. The interference regimes within and between these cavities are key to the spectral shaping of thermal emission. The radiative performances of the structures are evaluated by introducing a figure of merit. Using the example of a GaSb cell, it is shown that the structure can be optimized for providing the broadband large emission with a steep cutoff required for mitigating photoconversion losses.

OCIS codes: (030.5620) Radiative transfer; (290.6815) Thermal emission; (310.4165) Multilayer design.

References and links

1. N. P. Harder and P. Würfel, "Theoretical Limits of Thermophotovoltaic Solar Energy Conversion," Semicond. Sci. Technol. **18**(5), S151 (2003).
2. A. Datas and A. Martí, "Thermophotovoltaic Energy in Space Applications: Review and Future Potential," Sol. Energ. Mat. Sol. C. **161**, 285–296 (2017).
3. A. Lenert, D. M. Bierman, Y. Nam, W. R. Chan, I. Celanovic, M. Soljacic, and E. N. Wang, "A Nanophotonic Solar Thermophotovoltaic Device," Nature Nanotech. **1**, 1–5 (2014).
4. M. Shimizu, A. Kohiyama, and H. Yugami, "High-efficiency Solar-thermophotovoltaic System Equipped With a Monolithic Planar Selective Absorber/Emitter," J. Photonics Energy **5**(1), 053099 (2015).
5. C. Ungaro, S. K. Gray, and M. C. Gupta, "Solar Thermophotovoltaic System Using Nanostructures," Opt. Express **23**(19), A1149–A1156 (2015).
6. J. M. Bierman, A. Lenert, R. C. Walker, B. Bhatia, I. Celanovic, M. Soljačić, and E. N. Wang, "Enhanced Photovoltaic Energy Conversion Using Thermally Based Spectral Shaping," Nat. Energ. **1**, 16068 (2016).
7. O. Dupré, R. Vaillon, and M. A. Green, *Thermal Behaviour of Photovoltaic Devices. Physics and Engineering* (Springer, 2017).
8. D. L. C. Chan, M. Soljačić, and J. D. Joannopoulos, "Thermal Emission and Design in 2d-periodic Metallic Photonic Crystal Slabs," Opt. Express **14**(19), 8785–8796 (2006).
9. J. G. Fleming, S. Y. Lin, I. El Kady, and K. M. Ho, "All-metallic Three-dimensional Photonic Crystals With a Large Infrared Bandgap," Nature **417**, 52–55 (2002).
10. P. Nagpal, S. E. Han, A. Stein, and D. J. Norris, "Efficient Low-temperature Thermophotovoltaic Emitters from Metallic Photonic Crystals," Nano Lett. **8**(10), 3238–3243 (2008).

#313518 https://doi.org/10.1364/OE.26.004346
Journal © 2018 Received 15 Nov 2017; revised 18 Jan 2018; accepted 21 Jan 2018; published 9 Feb 2018

Optics EXPRESS

11. V. Rinnerbauer, Y. X. Yeng, W. R. Chan, J. J. Senkevich, J. D. Joannopoulos, M. Soljačić, and I. Celanovic, "High-temperature Stability and Selective Thermal Emission of Polycrystalline Tantalum Photonic Crystals," Opt. Express **21**(9), 11482–11491 (2013).
12. C. Arnold, F. Marquier, M. Garin, F. Pardo, S. Collin, N. Bardou, J. L. Pelouard, and J. J. Greffet, "Coherent Thermal Infrared Emission by Two-dimensional Silicon Carbide Gratings," Phys. Rev. B **86**, 035316 (2012).
13. A. Narayanaswamy and G. Chen, "Thermal Emission Control With One-dimensional Metallodielectric Photonic Crystals," Phys. Rev. B **70**, 125101 (2004).
14. I. Celanovic, D. Perreault, and J. Kassakian, "Resonant-cavity Enhanced Thermal Emission," Phys. Rev. B **72**, 075127 (2005).
15. N. P. Sergeant, O. Pincon, M. Agrawal, and P. Peumans, "Design of Wide-angle Solar-selective Absorbers using Aperiodic Metal-dielectric Stacks," Opt. Express **17**(25), 22800–22812 (2009).
16. E. Nefzaoui, J. Drevillon, and K. Joulain, "Selective Emitters Design and Optimization for Thermophotovoltaic Applications," J. Appl. Phys. **111**(8), 084316 (2012).
17. E. Blandre, P. O. Chapuis, and R. Vaillon, "Spectral and Total Temperature-dependent Emissivities of Few-layer Structures on a Metallic Substrate," Opt. Express **24**(2), A374–A387 (2016).
18. B. J. Lee and Z. M. Zhang, "Design and Fabrication of Planar Multilayer Structures With Coherent Thermal Emission Characteristics," J. Appl. Phys. **100**(6), 063529 (2006).
19. L. P. Wang, B. J. Lee, X. J. Wang, and Z. M. Zhang, "Spatial and Temporal Coherence of Thermal Radiation in Asymmetric Fabry-Pérot resonance cavities," Int. J. Heat Mass Transfer **52**(13–14), 3024–3031 (2009).
20. L. P. Wang, S. Basu, and Z. M. Zhang, "Direct Measurement of Thermal Emission From a Fabry–Pérot Cavity Resonator," J. Heat Transfer **134**, 072701 (2012).
21. G. E. Guazzoni, "High-temperature Spectral Emittance of Oxides of Erbium, Samarium, Neodymium and Ytterbium," Appl. Spectrosc. **26**(1), 60–65 (1972).
22. D. L. Chubb, A. T. Pal, M. O. Patton, and P. P. Jenkins, "Rare Earth Doped High Temperature Ceramic Selective Emitters," J. Eur. Ceram. Soc. **19**(13–14), 2551–2562 (1999).
23. B. Bitnar, W. Durisch, J. C. Mayor, H. Sigg, and H. R. Tschudi, "Characterisation of Rare Earth Selective Emitters for Thermophotovoltaic Applications," Sol. Energ. Mat. Sol. Cells **73**(3), 221–234 (2002).
24. N. A. Pfiester and T. E. Vandervelde, "Selective Emitters for Thermophotovoltaic Applications," Phys. Status Solidi (a) **214**(1), 1600410 (2017).
25. D. Chester, P. Bermel, J. D. Joannopoulos, M. Soljacic, and I. Celanovic, "Design and Global Optimization of High-efficiency Solar Thermal Systems With Tungsten Cermets," Opt. Express **19**(S3), A245–A257 (2011).
26. P. N. Dyachenko, J. J. do Rosário, E. W. Leib, A. Yu. Petrov, M. Störmer, H. Weller, T. Vossmeyer, G. A. Schneider, and M. Eich, "Tungsten Band Edge Absorber/Emitter Based on a Monolayer of Ceramic Microspheres," Opt. Express **23**(19), A1236–A1244 (2015).
27. P. N. Dyachenko, S. Molesky, A. Y. Petrov, M. Stormer, T. Krekeler, S. Lang, M. Ritter, Z. Jacob, and M. Eich, "Controlling Thermal Emission With Refractory Epsilon-near-zero Metamaterials via Topological Transitions," Nat. Comm. **11809**, (2016).
28. M. Chirumamilla, A. S. Roberts, F. Ding, D. Wang, P. K. Kristensen, S. I. Bozhevolnyi, and K. Pedersen, "Multilayer Tungsten-alumina-based Broadband Light Absorbers for High-temperature Applications," Opt. Mater. Express **6**(8), 2704–2714 (2016).
29. Z. Zhou, E. Sakr, Y. Sun, and P. Bermel, "Solar Thermophotovoltaics: Reshaping the Solar Spectrum", Nanophotonics **5**(1), 11 (2016).
30. J. H. Kim, S. M. Jung, and M. W. Shin, "High-temperature Degradation of One-dimensional Metallodielectric (W/SiO_2) Photonic Crystal as Selective Thermal Emitter for Thermophotovoltaic System", Opt. Mater. **72**, 45–51 (2017).
31. A. Kohiyama, M. Shimizu, and H. Yugami, "Unidirectional Radiative Heat Transfer With a Spectrally Selective Planar Absorber/Emitter for High-efficiency Solar Thermophotovoltaic Systems," Appl. Phys. Exp. **9**(11), 112302 (2016).
32. S. M. Rytov, I. U. A. Kravtsov, and V. I. Tatarskii, *Principles of Statistical Radiophysics: Elements of Random Fields* (Springer-Verlag, 1989).
33. D. Polder and M. Van Hove, "Theory of Radiative Heat Transfer Between Closely Spaced Bodies," Phys. Rev. B **4**, 3303–3314 (1971).
34. M. Francoeur, M. P. Mengüç, and R. Vaillon, "Solution of Near-field Thermal Radiation in One-dimensional Layered Media Using Dyadic Green's Functions and the Scattering Matrix Method," J. Quant. Spectrosc. Radiat. Transfer **110**(18), 2002–2018 (2009).
35. E. Palik, *Handbook of Optical Constants of Solids,* 1^{rst} *edition* (Academic University, 1987)
36. M. A. Kats, D. Sharma, J. Lin, P. Genevet, R. Blanchard, Z. Yang, M. M. Qazilbash, D. N. Basov, S. Ramanathan, and F. Capasso, "Ultra-thin Perfect Absorber Employing a Tunable Phase Change Material," Appl. Phys. Lett. **101**(22), 221101 (2012).
37. M. A. Kats, P. Genevet, R. Blanchard, and F. Capasso, "Nanometre Optical Coatings Based on Strong Interference Effects in Highly Absorbing Media," Nature Mater. **12**, 20–24 (2012).
38. C. Hägglund, S. P. Apell, and B. Kasemo, "Maximized Optical Absorption in Ultrathin Films and its Application to Plasmon-based Two-dimensional Photovoltaics," Nano Lett. **10**, 3135–3141 (2010).

Optics EXPRESS

39. M. Francoeur, M. P. Mengüç, and R. Vaillon, "Spectral Tuning of Near-field Radiative Heat Flux Between Two Thin Silicon Carbide Films," J. Phys. D: Appl. Phys **43**(7), 075501 (2010).
40. A. Bid, A. Bora, and A. K. Raychaudhuri, "Temperature Dependence of the Resistance of Metallic Nanowires of Diameter ≥15 nm : Applicability of Bloch-Grüneisen Theorem," Phys. Rev. B **74**(3), 035426 (2006).
41. M. Francoeur, R. Vaillon, and M. P. Mengüç, "Thermal Impacts on the Performance of Nanoscale-gap Thermophotovoltaic Power Generators," IEEE Trans. Ener. Conv. **26**(2), 686–698 (2011).
42. M. P. Bernardi, O. Dupré, E. Blandre, P. O. Chapuis, R. Vaillon, and M. Francoeur, "Impacts of Propagating, Frustrated and Surface Modes on Radiative, Electrical and Thermal Losses in Nanoscale-gap Thermophotovoltaic Power Generators," Sci. Rep. **5**, 11626 (2015).
43. J. DeSutter, M. P. Bernardi, and M. Francoeur, "Determination of Thermal Emission Spectra Maximizing Thermophotovoltaic Performance Using a Genetic Algorithm," Energ. Convers. Manage. **108**, 429–438 (2016).

1. Introduction

One of the key points for designing high-efficiency thermophotovoltaic (TPV) systems is to match the spectral emission of the radiator with the spectral range where photons are converted into electron-hole pairs (EHP) inside the photovoltaic (PV) device. In the case of solar-TPV devices, where the radiator is heated by sunlight radiation, achieving this spectral matching could allow getting closer to the theoretical efficiency limit of these systems, evaluated at 85% [1]. However, the maximum efficiency experimentally achieved for direct thermal-to-electricity energy conversion is around 25% [2], and only a few percents for solar-TPV systems [3–6]. This emphasizes that optimizing these systems is still a key topic of research to reach high-performance TPV devices. An efficient TPV radiator should have a large emission in the spectral range where the PV device converts photons into EHP, i.e. for photon energies above the bandgap of the PV cell. On the contrary, sub-bandgap photons do not generate EHP, but are absorbed by the lattice atoms and free carriers, generating heat that decreases the conversion performances of the PV device [7]. Therefore, sub-bandgap photons are detrimental to the overall efficiency, and the TPV radiator should have the lowest emission in this spectral range. In this frame, numerous studies dealt with the spectral thermal emission of selective emitters using different materials and geometries. Spectral selectivity was reported for two-dimensional [8] and three-dimensional photonic crystals [9–11], as well as for emitters with surface gratings [12]. However, more simple structures such as one-dimensional metallo-dielectric multilayer (or photonic crystals) structures showed a great potential for tailoring the spectral emission [13–17]. Spectral selectivity of such structures relies on Fabry-Pérot resonances that occur inside the transparent dielectric layers, allowing the increase or decrease of thermal emission for selected wavelengths with constructive and destructive interferences, respectively. Several experimental studies on the measurement of the thermal emission of few-layer structures reported this effect [18–20]. As for materials for TPV radiators, rare earth compounds were first considered due to their peculiar optical properties [21–24]. However, it is also necessary to ensure the thermal stability of the radiator in order to keep the same spectral emission at its operating temperature, meaning that it should be thermally stable. The assessement of thermal stability of radiators at high temperature is a growing topic, and it appears that refractory metals, such as molybdenum and tungsten, are efficient materials due to their high melting point [4, 9, 10, 15, 25–30]. Eventually, simple structures give the advantage of easiness of fabrication and higher thermal stability. It can be summarized that efficient and sustainable thermophotovoltaic energy conversion devices require easy-to-fabricate, high-temperature, thermally-stable radiators.

For the reasons listed above, we investigate in this paper the thermal emission of one-dimensional metallo-dielectric trilayer-on-substrate structures, where the refractory metal is molybdenum and the transparent layers are made of hafnium oxide (or hafnia). These structures were already tested in a solar-TPV system and proven to be efficient TPV radiators [31]. If the ground principles of the physical effects occurring in these structures are known for structures with one layer deposited on a substrate, it is not entirely the case for complex structures with several layers. We therefore

Optics EXPRESS

provide in the first part an extended analysis of the specific interference phenomena occurring in such a trilayer on substrate structure. We highlight that in addition to its high melting point, Mo is a good material for TPV radiators because of its intrinsic spectral selectivity due to the transition between intraband and interband absorption. The analysis of multireflections in these spectral regions allows to understand the different interference patterns. The study of the behavior of the thermal emission of such structures is also extended by decoupling contributions of the forward and backward waves emitted by the Mo film. In particular, we show that they interfere and contribute significantly to shaping the spectral emissivity of the structure. In a second step, we demonstrate that it is possible to optimize the thermal emission of these structures for a given TPV application, by matching the thermal emission of the structure with the bandgap of a GaSb cell. To do so, we introduce a figure of merit and show the impact of the architecture on the definition of the figure of merit.

2. Methodology

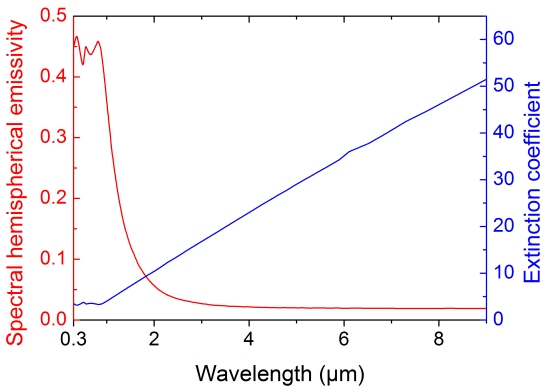

Fig. 1. Spectral values of the extinction coefficient of Mo (blue line) and spectral hemispherical emissivity of a Mo substrate (red line).

Thermal emission of the trilayer-on-substrate structures is calculated using fluctuational electrodynamics [32]. Maxwell's equations are solved by means of dyadic Green's functions, and the thermally generated electromagnetic currents are given by the Fluctuation-Dissipation Theorem [33]. The Weyl components of the Green tensors are calculated using the S-matrix method [34]. This approach consists in calculating four coefficients, corresponding to the amplitude of the waves emitted in the forward and backward directions and traveling in the forward and backward directions. It is worth mentioning that the S-matrix method has the advantage to allow analyzing the contributions of the forward and backward emitted waves by a layer of the structure, which cannot be done straightforwardly in other approaches based on the calculation of the absorption, such as RCWA (rigorous coupled wave approximation). Once the spectral emissive power of the structure is calculated, the spectral hemispherical emissivity is obtained by dividing it by that of the blackbody, given by Planck's law, at the same temperature.

Two materials intentionnally selected in this work are considered: molybdenum (Mo), a refractory metal, and hafnium oxide (HfO_2), a dielectric material. Both materials are good choices for high-temperature TPV radiators because of their high melting point. The spectral values of the optical indices of both materials are provided in [35] at room temperature. Variations of optical indices with temperature, likely to take place between room temperature and the operating temperature of a TPV radiator (around 1500 K), are not accounted for. HfO_2 has a

Optics EXPRESS

low extinction coefficient in the infrared, and is therefore transparent. Thus, it is expected that multireflections can occur inside hafnia layers, leading to interferences phenomena that could allow controlling the emission spectrum. The spectral values of the extinction coefficient of Mo are reported in Fig. 1. Two spectral regions are exhibited. Between 0 and 1 μm, the extinction coefficient does not vary much and takes values around 3.5 (close to the real part of the refractive index). In this spectral range, the absorption of photons is dominated by electronic transitions from the d-band to the s-band (interband transitions). Above 1 μm, the extinction coefficient increases. In this regime, the absorption is dominated by electronic intraband transitions. The existence of these two extinction regimes impacts the spectral emission of Mo, as illustrated in Fig. 1, where the spectral hemispherical emissivity of a single Mo substrate is displayed. It is observed that the spectral emission follows the spectral variations of the optical indices: in the interband transition region, the spectral emissivity of Mo is moderate, taking values around 0.4. As its extinction coefficient increases, Mo becomes more and more reflective and its emission consequently decreases. In the end, due to the transition between interband and intraband absorption, a single Mo substrate already has interesting intrinsic emission properties for thermophotovoltaics. Indeed, it exhibits a broadband emission with a steep cutoff.

3. Analysis of interference phenomena in a Mo-HfO_2 trilayer on substrate structure

To get closer to the ideal emission for TPV applications, it is necessary to enhance the moderate spectral hemispherical emissivity of Mo below the cutoff wavelength while keeping it close to 0 for large wavelengths. As shown in [14, 16–20], transparent layers of selected thicknesses can act as amplifiers of a layer emission by means of Fabry-Pérot interferences. Following the framework of [16, 17], we consider a structure consisting of two resonant HfO_2 layers separated by a 10 nm thin Mo layer, and deposited on a Mo substrate (schematic in Fig. 2(a)). The thickness of the Mo layer is chosen to be as small as possible such that waves can be transmitted through it, but not smaller than 10 nm in order to avoid dealing with variations of the dielectric function due to increased collision frequency of electrons and phonons at the boundaries of the layer [40]. Considering the thickness of the two HfO_2 layers to be equal to t, the spectral hemispherical emissivity of the structure is reported in Fig. 2(b) as a function of t. The colormap exhibits branches of large values of spectral hemispherical emissivity that are a signature of the constructive interferences occurring due to multireflections inside the oxide layers. It is worth noticing that for a thickness of 50 nm (represented by the horizontal dashed line on the emissivity map), the spectral hemispherical emissivity exhibits values close to 1 below 1 μm, and a low emission above, which is close to the ideal emission. Optimization of the radiator architecture and quantification of its performances for TPV applications will be discussed in the last section of this paper.

We first investigate the behavior of interferences and their impact on the spectral hemispherical emissivity. As mentioned previously, the emission of Mo layers are amplified by Fabry-Pérot interferences. However, even for wavelengths larger than 1 μm, the spectral hemispherical emissivity along the constructive interference branches takes large values. In this spectral region, the Mo-HfO_2 interface is very reflective due to the large contrast of optical indices between Mo and hafnia. It induces that a lot of multireflections occur inside the HfO_2 layers, leading to a large amplification of the emission due to interferences [17]. On the other hand, for wavelengths below 1 μm, the reflection coefficient of the Mo-HfO_2 interface is moderate, because the optical indices of both materials are close. Still, the spectral hemispherical emissivity takes large values too. It was highlighted in [36, 37] that strong absorption does not necessarily need large reflection coefficients and typical quarter-wavelength resonances associated to Fabry-Pérot interferences. It can also be achieved for specific phase lags of the reflection coefficients at the material interfaces, leading to another type of interferences in subwavelength films. In particular, it was shown

Optics EXPRESS

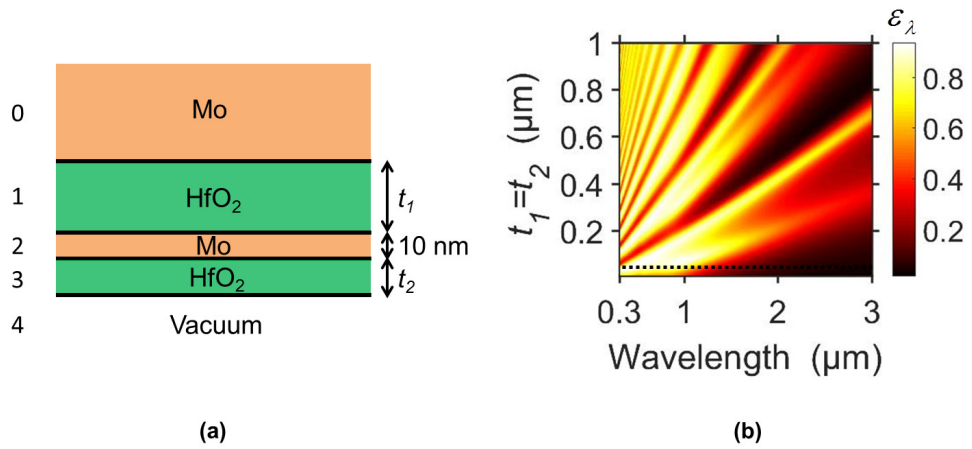

Fig. 2. (a) Schematic of the few-layer structure under consideration. (b) Spectral hemispherical emissivity of the structure as a function of the thickness of the oxide layers, t_1 being equal to t_2.

that strong absorption occurs if the real and imaginary parts of the optical index of a thin layer sandwiched between lossless materials are of the same order of magnitude [38]. To investigate if such phenomena are possible in our Mo-based structures, we analyze the partial reflectivity of a simplifed configuration, where layer 3 is removed (acting only as a further amplifier in [17]) and the thickness of the remaining HfO_2 layer is fixed to 100 nm. The partial reflectivity r_l, function of the number of secondary waves l, is defined as [36]

$$\begin{aligned} r_0 &= R_2 \\ r_l &= T_2 \times r_{10}^{l} \times R_2^{l-1} \times T_2 \times e^{2lik_{z_2}t_1},\ l = 1,\ 2,\ 3,\ 4... \end{aligned} \tag{1}$$

where R_2 and T_2 are the global reflection and transmission coefficients of the Mo thin film that take the form [39]

$$R_2 = \frac{r_{12} + r_{23}e^{2ik_{z_2}d}}{1 + r_{12}r_{23}e^{2ik_{z_2}d}}, \tag{2}$$

$$T_2 = \frac{t_{12} + t_{23}e^{ik_{z_2}d}}{1 + r_{01}r_{12}e^{2ik_{z_2}d}}. \tag{3}$$

Here, r_{ij} and t_{ij} are the Fresnel reflection and transmission coefficients at the interface between medium i and j, and k_z is the component of the wavevector perpendicular to the interface. d is the thickness of the Mo layer (10 nm). The infinite sum of r_l corresponds to the total reflectivity of the structure.

In Fig. 3, we report the sum of partial reflectivities $r_0 + r_1 + ... + r_l$ of the considered structure as a function of the number of secondary waves l, for two wavelengths located in the two different spectral regions: $\lambda = 0.3$ μm (Fig. 3(a)) and $\lambda = 10$ μm (Fig. 3(b)). The inserts in Fig. 3 represent the successive positions of the sum of partial reflectivities in the complex plane, which tends ultimately to the total complex reflectivity of the system. It can be seen that for $\lambda = 0.3$ μm, the sum of partial reflectivities converges to the value of the total reflectivity for a small number of secondary waves. The total reflectivity is low, therefore strong emission is achieved. As the optical path is small, the variations of the sum of the partial reflectivities are guided by the phase

Optics EXPRESS

lags induced by reflections at the interfaces. This is highlighted by the large angle between two successive phasors (sum of partial reflectivities) in Fig. 3(a). On the contrary, for $\lambda = 10$ µm, the sum of partial reflectivities converges slowly to its final value, due to the large value of the reflection coefficient of the Mo-HfO_2 interface. In this second case the phase lag is accumulated by travelling, requiring a lot of round trips inside the different layers to get strong interference effects. Such effect can lead to strong reflectivity, as shown in Fig. 3(b), but also to strong emission, as shown by the resonances in Fig. 2(b) for wavelengths larger than ≈ 2 µm. This is similar to the results reported in [17]. As a conclusion of this section, we have shown that two different regimes of interferences occur in the Mo-based structures: in both low-wavelength and high-wavelength ranges, high values of the spectral hemispherical emissivity can be reached.

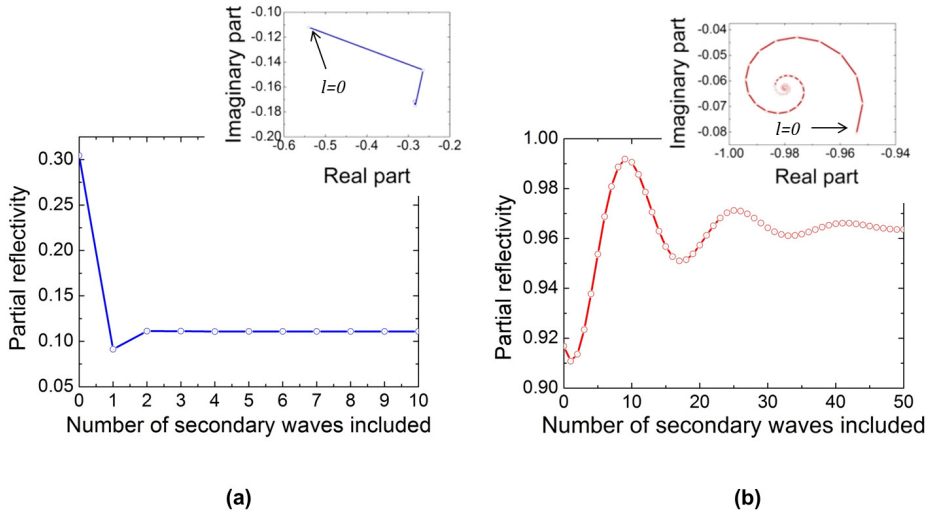

Fig. 3. Sum of partial reflectivities $r_1 + r_2 + ... + r_l$ as a function of the number of secondary waves l for $t_1 = 100$ nm. (a) $\lambda = 0.3$ µm, (b) $\lambda = 10$ µm. The inserts represent the sum of partial reflectivities in the complex plane.

In the following section, we discuss the origin of the interference branches that can be seen in Fig. 2(b). It can be observed that the branches are paired, and we test the hypothesis that in each pair, an interference branch is caused by resonances induced by each of the two HfO_2 layers. To check this, we analyze the contribution of the emission of the Mo film to the structure. More specifically, we analyze the contributions of the forward and backward emitted waves. By fixing the coefficients corresponding to the amplitudes of the forward (backward) emitted waves to 0, we can analyze the contribution of the backward (forward) emitted waves to the emission. The results are gathered in Fig. 4. It is observed that for each pair of branches, the lower one has a larger intensity when considering forward emitting waves. On the other hand, when considering backward emitted waves, the higher branch has a larger intensity. Since backward emitted waves have to be reflected one less time to reach the interface between medium 2 and medium 1, we conclude that the higher branch are due to interferences in the upper HfO_2 layer. Following the same reasoning, the lower branch corresponds to interferences in the lower HfO_2 layer. It is also worth noticing that the incoherent addition of the forward and backward emitted waves (Fig. 4(c)) is lower than the total emission of the Mo film inside the structure (Fig. 4(d)). Therefore, it is clear that backward and forward waves emitted by the thin film interfere, and that this interference scheme plays a major role in shaping the emission spectrum of the structure. In

Optics EXPRESS

the case of a single emitting substrate, only forward emitted waves participate to the emission. Therefore, the presence of the emitting film enhances the impact of interferences. To validate the hypothesis mentioned before, we analyze the constructive interference conditions of the structure. We assume that the first resonator comprises layers 1 and 2, and the second layers 2 and 3 (as depicted in Fig. 5). Note that in this case, the thin Mo film contributes to the interference patterns. The constructive interference conditions can be retrieved by analyzing the phase lag of waves between two round trips from one edge of the resonator to the other. Phase lag can occur due to the difference of optical path lengths, and because of reflections at the interfaces. By equalizing the sum of the phase lags to $2m\pi$, where m is an integer, the constructive interference conditions on the thickness of the layer t and the wavelength λ take the form:

$$t = \left(m - \frac{\arg\left(r_{10}\right) + \arg\left(R_2\right)}{2\pi} \right) \frac{\lambda}{2n\cos\varphi} \tag{4}$$

for the first resonator, and

$$t = \left(m - \frac{\arg\left(R_2\right) + \arg\left(r_{34}\right)}{2\pi} \right) \frac{\lambda}{2n\cos\varphi} \tag{5}$$

for the second one. Here, φ is the angle of incidence of waves inside hafnia layers, n is the refractive index of hafnium oxide ($n \approx 2$), and the argument of the reflection coefficient is related to the phase lag induced by a reflection at this interface.

The contribution of normal waves to the spectral hemispherical emissivity as a function of the thickness of the HfO_2 layers considering $t_1 = t_2$ is reported in Fig. 5. The dashed and solid lines represent the theoretical constructive interference conditions related to the two resonators mentioned earlier (dashed for resonator 1 and solid for resonator 2). A good match is observed between the high-emissivity branches in the contour map of the spectral hemispherical emissivity and the theoretical constructive interference conditions for wavelengths larger than 1 μm. As predicted, in each pair one branch is related to one resonator. Below 1 μm, the high-emissivity branches and the theoretical interference conditions start to depart from each other. Again, this is related to variations of the optical properties of Mo around this wavelength. For wavelengths larger than 1 μm, the Mo-HfO_2 interface is very reflective, such that it can be assumed that multireflections can occur in one resonator only. However, for wavelengths smaller than 1 μm, waves can be transmitted through the Mo layer more easily, and multireflections can occur in both resonators. The constructive interference conditions calculated before are therefore not relevant anymore, hence the resulting mismatch. Summarizing this section, we have analyzed the origin of the spectral hemispherical emissivity of the studied structure. We have highlighted different spectral regimes of interferences corresponding to the two regimes of absorption of Mo. The origin of each interference branches in the emissivity map has been explained. In the next section, we demonstrate that the design of a TPV radiator using this structure is possible.

4. Design and optimization of the structure for a selected TPV application

A good radiator for a TPV system with a GaSb cell should have the largest emissivity possible below the wavelength corresponding to the bandgap of GaSb (at 300 K, $E_g^{\mathrm{GaSb}} = 0.7$ eV, $\lambda_g^{\mathrm{GaSb}} = 1.7$ μm), and the lowest emissivity possible above. Mo, due to its transition between interband and intraband absorption around this wavelength, is a good choice for this application, as a large broadband emission with a steep cutoff can be obtained with the Mo-HfO_2 trilayer-on-substrate structure introduced previously. In this section, we optimize the efficiency of the emitter for this TPV application. To do so, we first define a function ψ that represents the deviation to the ideal emission

$$\psi\left(\lambda\right)) = \begin{cases} q_\lambda^{bb}(T)\left(1-\epsilon_\lambda\right) & \text{for} \lambda \le \lambda_g \\ q_\lambda^{bb}(T)\epsilon_\lambda & \text{for} \lambda > \lambda_g \end{cases}, \tag{6}$$

Optics EXPRESS

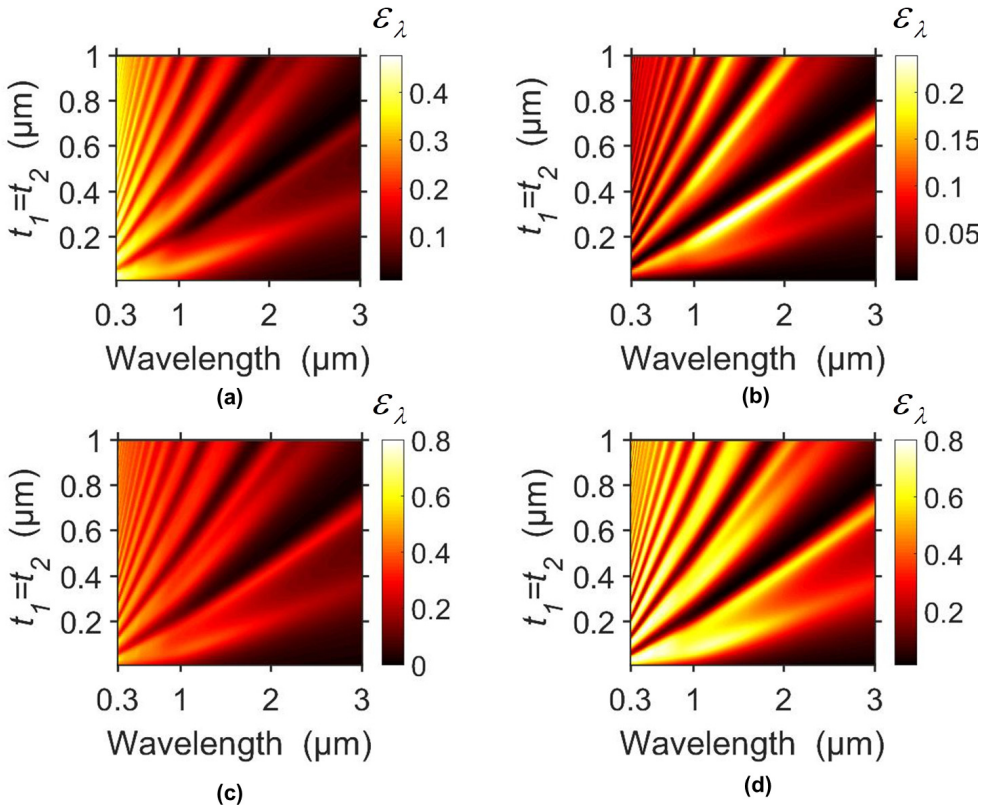

Fig. 4. Contribution of the Mo film to the spectral hemispherical emissivity of the structure considering $t_1 = t_2$. (a) considering only forward emitted waves. (b) considering only backward emitted waves. (c) incoherent addition the contribution of forward and backward emitted waves. (d) considering the coherence between every type of waves.

where $q_\lambda^{bb}(T)$ is the spectral emissive power of a blackbody at temperature T, and ϵ_λ is the spectral hemispherical emissivity. In solar-TPV experimental demonstrators, a temperature of 1500 K can typically be achieved with such structures [31]. At this temperature, the wavelength where the blackbody intensity is maximum ($\lambda_{\max}(1500\ \mathrm{K}) = 1.93\ \mu\mathrm{m}$) is close to the wavelength corresponding to the bandgap of GaSb at 300 K. Therefore, we choose this value for the temperature in the following. The same procedure can of course be applied for other radiator temperatures. The function ψ represents the fraction of energy that is below the ideal emission for wavelengths below the cutoff, and the fraction of energy that is above the ideal emission for wavelengths above the cutoff. A figure of merit can be defined as follows:

$$FOM = 1 - \frac{\int_{\lambda_{\min}}^{\lambda_{\max}} \psi(\lambda)\, d\lambda}{\int_{\lambda_{\min}}^{\lambda_{\max}} q_\lambda^{bb}(T)\, d\lambda}. \tag{7}$$

where $\lambda_{\min}$ and $\lambda_{\max}$ are the smallest and largest values of wavelengths for which the optical indices are provided in [35]. In the worst case where the emission is 0 below the cutoff in wavelength and 1 above it, function ψ is exactly the blackbody spectrum and the figure of merit is 0. For an optimal spectral hemispherical emissivity, it takes the value 1. Therefore, the figure

Optics EXPRESS

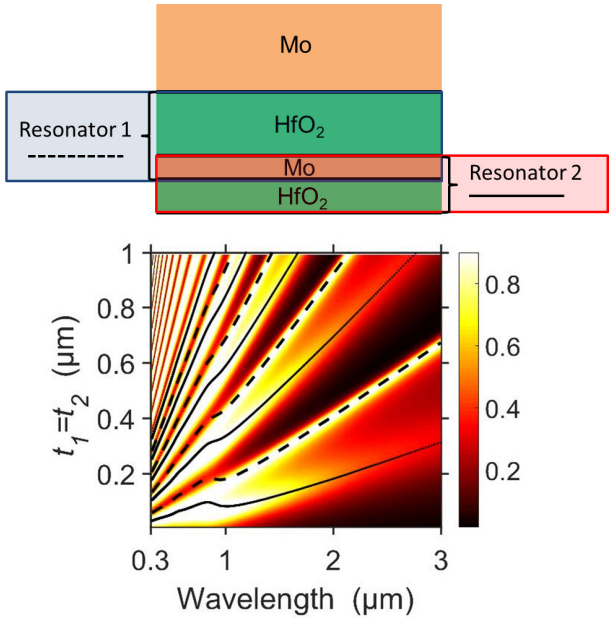

Fig. 5. Spectral emissivity of the trilayer-on-substrate structure with normal incidence. The dashed and solid lines represent the constructive interference conditions at normal incidence of the two Fabry-Pérot resonators highlighted above.

of merit is a number between 0 and 1 and represents the fraction of emitted energy useful for TPV energy conversion.

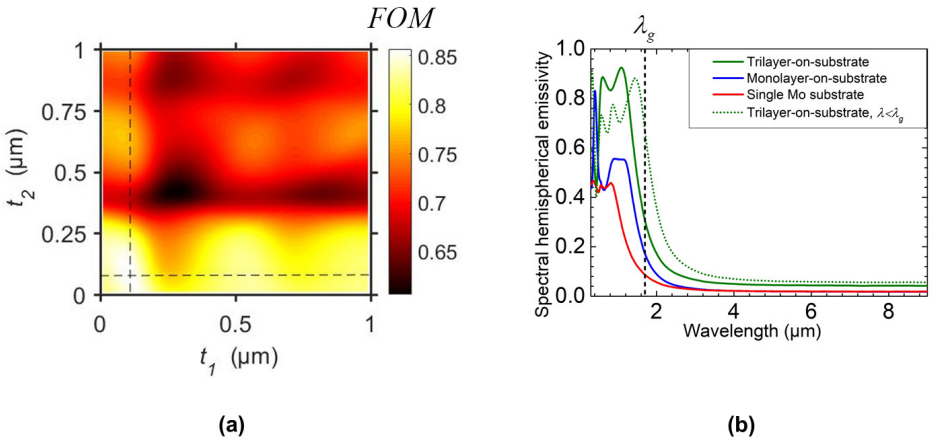

Fig. 6. (a) Figure of merit of the structure as a function of the thicknesses of the hafnium oxide layers t_1 and t_2. (b) Spectral hemispherical emissivity of the single Mo substrate (red line), of the optimized monolayer-on-substrate structure (blue line) and of the optimized trilayer on substrate structure (green line). The dashed curve corresponds to the optimization for $\lambda < \lambda_g$ only. The dashed vertical line represents the wavelength corresponding to the bandgap of GaSb at 300 K.

Optics EXPRESS

In Fig. 6, we report the values of the figure of merit as a function of the size of the two HfO_2 layers. The figure of merit exhibits peaks and dips with multiple local maxima. When increasing the thickness of one of the two layers, the constructive interference peaks shift toward larger wavelengths. The peaks and dips are due to the peaks of different orders that pass through the zone where the emission is expected to be maximum as the thickness increases. Even if local maxima are exhibited, a maximum figure of merit of 0.85 is found for $t_1 = 110$ nm and $t_2 = 80$ nm. For this architecture, the spectral hemispherical emissivity of the structure is plotted in Fig. 6(b). As expected it exhibits a large broadband emission with a steep cutoff around the wavelength corresponding to the bandgap of GaSb, which is close to the ideal emission defined earlier. Hence, we have demonstrated that the structure under consideration is efficient for TPV applications. It is also worth mentioning that emission of these structures is quasi-isotropic [17]. We also plotted in Fig. 6(b) the spectral hemispherical emissivity of the architecture maximizing the figure of merit for a structure composed with a single resonator deposited on a Mo substrate (layers 0 and 1 only) and of a single Mo substrate. The amplification of the emission of the Mo substrate due to the successive addition of resonant layers is clearly depicted. This was already discussed in [17]. Eventually, it should be noted that to maximize the energy yield by the TPV system, the only criterion is that the spectral hemispherical emissivity of the structure should be maximum for wavelengths below the cutoff. As a consequence, the integrals in Eq. (7) should be performed from $\lambda_{\min}$ to λ_g. In this case, the architecture maximizing the figure of merit is different from the previous one, and its resulting spectral hemispherical emissivity is plotted in Fig. 6(b) (dashed line). The impact of the absorbed photons that are not converted could be accounted for more accurately by introducing spectral weight in the function $\psi(\lambda)$, which would consider their negative impact. This would require solving the full coupling with the charge transport and the thermal field, as in [41–43].

5. Conclusions

We have studied the thermal emission of trilayer structures made of hafnia and Mo layers deposited on a Mo substrate, which resist to high temperatures. Mo has been selected because of the spectral variations of its optical properties due to the transition between interband and intraband absorption mechanisms, which are particularly interesting for TPV applications. We then have analyzed the different specific regimes of interferences in the structure arising from the spectral variations of the reflection and transmission coefficients at the Mo-hafnia interfaces. It is worth noticing that highly-reflective interfaces are not the only way to reach high-emission: very high absorption can be achieved using materials with optical indices of the same order of magnitude. The origin of the interference peaks has been explained by means of the analysis of the forward and backward emission of waves by the Mo film, and by determining the condition for constructive interferences inside the structure. Each hafnia layer is responsible for its own interference peaks in the spectral region where the Mo-hafnia layer is highly reflective. If the reflection coefficient of this interface is moderate, waves can easily cross the Mo thin layer, and be multireflected in the whole structure. It is key to note that forward and backward emitted waves by the film interfere. As a consequence, the presence of a thin film, whose forward and backward emitted waves participate to the emission, is key to enhance the impact of interferences. Eventually, we have evaluated the efficiency of this structure as a radiator for TPV applications. We have defined a figure or merit that can reach 85 % for the optimal architecture. As a summary, we have provided an in-depth explanation of the thermal emission of such structures and a guideline to optimize their emission for TPV applications. A future improvement should be to consider the variations with temperature of the optical indices of both materials, in order to calculate the thermal emission at the operating temperature of the radiator. Indeed, the extinction coefficient and refractive index provided in [35] are measured at ambient temperature. It is expected that the optical properties of hafnia do not vary much with temperature. However, it

Optics EXPRESS

has been shown for noble metals such as aluminum that the thermal emission increases with temperature due to the increase of electron-phonon scattering processes - even if the overall emission of noble metals remains low [17]. We should also mention that the criterion for the ideal emission does not account for thermal effects. High energy photons can be detrimental because they generate heat through thermalization, which can decrease the performances of the PV cell. A previous study [43] showed that an improved spectral emissivity for TPV systems is in fact a band spectrum when taking into account thermal effects. However, the spectral position of the second cutoff at lower wavelength requires an in-depth analysis of the impact of temperature on the performances of the PV device, which is not the scope of the this paper.
The structures presented in this article have already been tested in a solar-TPV system [31]. If in addition they confirm high temperature thermal stability, they would be fully validated for use in TPV applications. Therefore, the work provided by this paper represents a step toward high-efficiency TPV systems.

Funding

French National Research Agency (ANR) (ANR-16-CE05-0013); INSA Lyon BQR REDCAV.